Paper 54

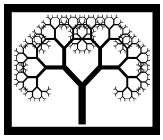

Proceedings of the Eleventh International Conference
on Computational Structures Technology,
B.H.V. Topping, (Editor),
Civil-Comp Press, Stirlingshire, Scotland

Impact Resistance of Metallic Cellular Materials: Effects of Cell Shape and Base Material Ductility

E. Law, K.K. Tan, S.D. Pang and S.T. Quek
Department of Civil and Environmental Engineering
National University of Singapore, Singapore

Abstract

Cellular materials are becoming increasingly popular for protection against impact and blast as they are lightweight yet able to absorb large amounts of energy but transmit relatively low forces to the protected object. In this paper, finite element simulations are carried out to investigate the effects of cell shape and base material ductility on the impact force and energy absorption capacity of metallic cellular materials with different relative densities subject to medium velocity impact. The results show that cell shape has a very significant influence on the overall response, with square cells resulting in the highest overall stress and energy absorption capacity followed by triangular, hexagonal and rhombic cells. Also, the effect of base material ductility is minimal at very low relative densities but rather considerable in cases with higher relative densities.

Keywords: finite element method, metallic honeycombs, dynamic crushing, energy absorption, medium velocity impact.

1 Introduction

Cellular materials – which can be defined as materials with complex internal topologies and an extremely high content of voids ranging from 50 to 90 per cent – are popular in their use as protective materials against impact as they are lightweight yet able to absorb large amount of impact energy with relatively low and stable impact force on the protected object. Due to these advantages, cellular materials have the potential to serve as feasible alternatives to conventional materials such as monolithic steel, concrete and polymeric foams in protective structures. The effectiveness of cellular materials for protection against impact loading is evident in natural materials such as fruit skins [1] and animal shells [2, 3]. It is well known that the mechanical response of such materials is highly dependent on their internal

topologies, and the use of cellular materials in the form of metallic foams and hexagonal honeycombs as core materials in sandwich panels has been investigated rather extensively, e.g. [4-7].

The mechanics of cellular materials under uniaxial compression have been studied by Gibson and Ashby [8], in which the response of cellular materials with honeycomb topologies under quasi-static loading can be divided into three regimes: an initial linear-elastic stage before yielding, a plateau stage in which the applied force remains relatively constant due to formation of plastic hinges during the collapse of cell walls, and the densification stage where the applied force increases rapidly after complete collapse of the cells. Qiu *et al*. [9], Wang and McDowell [10], and Ren and Silberschmidt [11] investigated the quasi-static response of planar lattices with different cell shapes and found that those which resist loading through axial resistance of cell walls – such as those with triangular and Kagome cells – have the highest stiffness-to-weight and strength-to-weight ratios. For cellular materials under dynamic compression, Qiu *et al.* [12] found that those with square and triangular cells result in the highest impact stress compared to those with hexagonal and rhombic cells.

Apart from regular lattices, the dynamic response of cellular materials with irregular topologies has also been studied by a number of researchers. Li *et al*. [13] reported that at low impact velocities both the existence of irregular cell shapes and the presence of non-uniform cell wall thickness reduce the plateau stress and energy absorption compared to cases with perfectly ordered hexagonal cells with uniform cell wall thickness. Furthermore, the effect of cell wall thickness uniformity seems to be more significant than cell shape irregularity, but these effects become less considerable with increasing impact velocity. A study by Adjari *et al*. [14] suggested that cell shape irregularity does not have a considerable effect on energy absorption. However, the effect of a missing cell cluster is also considered in their study which shows that the energy absorption does not change significantly with a missing cell cluster as large as 5 per cent, but one with a missing cell cluster of 10 per cent has considerably lower energy absorption compared a regular honeycomb with no defect. Moreover, Adjari *et al*. [14] also reported that the energy absorption capacity of honeycombs with lower relative densities is more sensitive to the presence of a defect.

Zhang *et al*. [15] showed that defects in the form of missing cell walls have considerable effects on a regular honeycomb under dynamic compression. The plateau stress is reported to reduce almost linearly with increase in local defect ratio (which is used to quantify the number of missing cell walls), and this effect is more significant when the defects are located along shear bands in the cellular material which would be formed in the absence of these defects. On the other hand, the overall deformation mode is altered only when the defects are located outside the regions along which these shear bands would be formed in the absence of the defects.

Therefore, the above mentioned studies show that the mechanical behavior of cellular materials depends significantly on the internal topology, specifically the shape of the cells as well as defects or irregularities in the cell shape and cell wall thickness. Yet, despite the focus and considerable effort in current and past research

to establish basic understanding on the mechanical properties of cellular materials, it has yet to be proven that hexagonal honeycombs (including those with irregular cell shapes and cell wall thickness) are the most effective form of cellular materials for impact protection compared to other shapes. Also, past studies have been mainly conducted for honeycombs with very low relative densities of around 10 per cent but the behavior of these materials with higher relative densities has not been widely investigated. Moreover, while there have been several studies on the effects of geometrical imperfections on the impact resistance of cellular materials, the effects of material imperfections such as base material ductility have not been considered so far; the base materials of these honeycombs are assumed to be elastic-perfectly plastic and of uniform strength throughout in past numerical investigations. Consequently, a more thorough examination of these factors on the impact resistance of cellular materials is necessary in order to design for optimum performance in various applications.

These issues are addressed in this study in which finite element simulations are carried out to investigate the mechanical response of metallic cellular materials under medium velocity impact. In particular, the effects of cell shape and base material ductility on the impact force and energy absorption capacity of these materials with different relative densities shall be examined.

2 Finite element model

Figure 1 shows the two-dimensional plane strain finite element model used in this study. A representative volume of the cellular material with length L = 100 mm and nominal width W = 100 mm is placed between two rigid plates with nominal thickness of 5 mm; the actual specimen width W depends on the shape and size of the cells. Due to symmetry, the analysis is performed using the left half of the cellular specimen only; the nodes along the line of symmetry as shown in Figure 1 are constrained from any horizontal displacement. The bottom plate is kept stationary while the top plate is used to compress the cellular specimen at a constant velocity v = 20 m/s in the y-direction. The left (unbounded) edge of the cellular specimen is free to displace in the x-direction but constraints are imposed such that it remains vertical. Contact between the specimen and the rigid plates as well as self-contact between the cell walls in the specimen are treated as frictionless.

The material properties of aluminum are used for the base material of the cellular specimen, which is assumed to be elastic-perfectly plastic up to the onset of rupture with mass density of 2700 kg/m^3, Young's modulus of 69 GPa, Poisson's ratio of 0.33, and yield strength of 103 MPa. Unless otherwise stated, the material plastic rupture strain ε_f (henceforth called the failure strain or ductility limit) is taken as 0.3. The material strain rate effect is taken into account by scaling the yield stress with a factor of $[1+(\dot{\varepsilon}/C)^{1/p}]$ following the Cowper-Symonds model, where $\dot{\varepsilon}$ is the strain rate while the Cowper-Symonds constants C and p are taken as 6500 s^{-1} and 4 respectively [16]. The cellular specimen is discretized using bilinear quadrilateral and constant strain triangular elements.

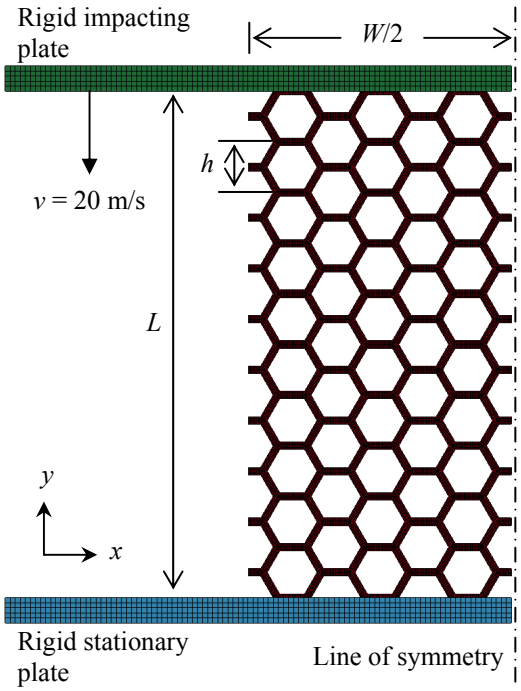

Figure 1. Finite element model of cellular specimen under dynamic uniaxial compression

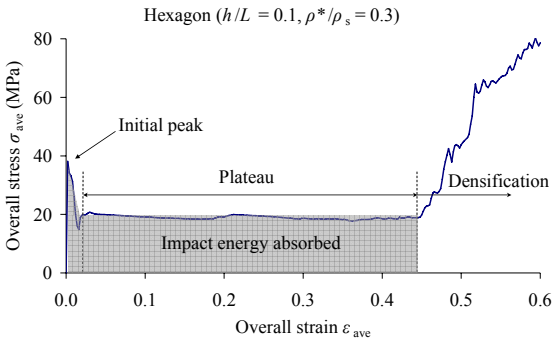

Figure 2. Typical overall stress-strain response of cellular specimen under dynamic uniaxial compression

Figure 2 shows the typical overall stress-strain response of the cellular specimen, in which the overall stress σ_{ave} is defined as the impact force exerted on the specimen divided by its initial nominal width $W/2$ while the overall strain ε_{ave} is taken as the total deformation in the direction of loading divided by initial length L. The three deformation regimes mentioned by Gibson and Ashby [8] are clearly displayed in Figure 2. In this study, the plateau stress is defined as the average overall stress within the plateau stage, while the impact energy absorbed is taken as

the area under the overall stress-strain response up to the onset of densification. The relative density ρ^*/ρ_s is defined as the density of the cellular specimen divided by density of a solid block of the same overall size made of the same base material [8].

3 Overall response of cellular materials with different cell shapes

3.1 Deformation mode

Figure 3 shows that deformation in cellular materials with hexagonal cells occurs through the formation of diagonal shear bands. This is because a hexagonal cell is able to deform more easily under inclined shear compared to vertical compression, since fewer plastic hinges are required to form a failure mechanism in the former compared to the later. Within the diagonal shear bands, rotation of plastic hinges happens at the joints between the cell walls; the plastic hinges are formed at both ends of the diagonal cell walls. With further compression, densification of the diagonal shear bands occurs when the cells within these bands collapse. Consequently, during the plateau stage, deformation in cellular materials with hexagonal cells is mostly localized within the shear bands and impact energy is mainly absorbed through the rotation of the plastic hinges in these shear bands.

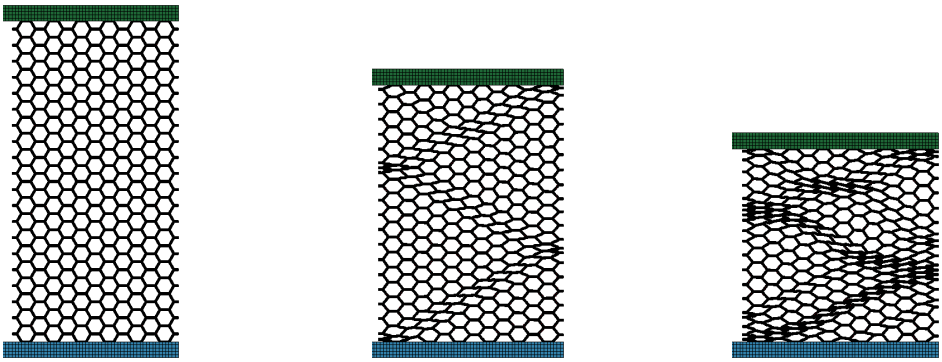

(a) $\varepsilon_{ave} = 0$ (b) $\varepsilon_{ave} = 0.2$ (c) $\varepsilon_{ave} = 0.4$

Figure 3. Deformation of cellular material with hexagonal cells of $\rho^*/\rho_s = 0.3$

Figure 4 shows that deformation in cellular materials with rhombic cells occurs through rotation of plastic hinges which are formed readily at the joints between cell walls because the orientation of the rhombic cells with respect to the direction of compression results in an inherent collapse mechanism. Thus, cellular materials with rhombic cells also absorb impact energy mainly through rotation of plastic hinges. However, unlike the case with hexagonal cells there is no clear formation of shear bands in the specimen; the material is rather evenly deformed throughout the

specimen. This is because the same number of plastic hinges is required to form a failure mechanism under both inclined shear and vertical compression for a rhombic cell. Therefore, since the cells are compressed vertically, they also collapse in the same direction.

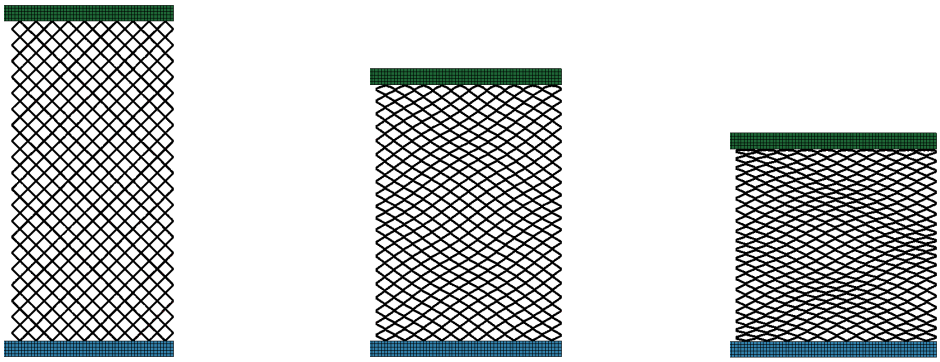

(a) $\varepsilon_{ave} = 0$ (b) $\varepsilon_{ave} = 0.2$ (c) $\varepsilon_{ave} = 0.4$

Figure 4. Deformation of cellular material with rhombic cells of $\rho^*/\rho_s = 0.3$

Cellular materials with square cells exhibit different collapse patterns in specimens with different relative densities. In specimens with low relative density, deformation generally initiates at the impact end and subsequently propagates towards the far end of the specimen as shown in Figure 5. Collapse of the square cells in these cases occurs through buckling of the vertical cell walls and formation of plastic hinges within these buckled cell walls. Thus, the impact energy is absorbed mainly through rotation of these plastic hinges. On the other hand, deformation is fairly uniform throughout the specimen in cases with high relative density as shown in Figure 6. Instead of cell wall buckling, the dominant mode of deformation and energy absorption is squashing or crushing of the vertical cell walls since the cell wall length-to-thickness ratio decreases with higher relative density.

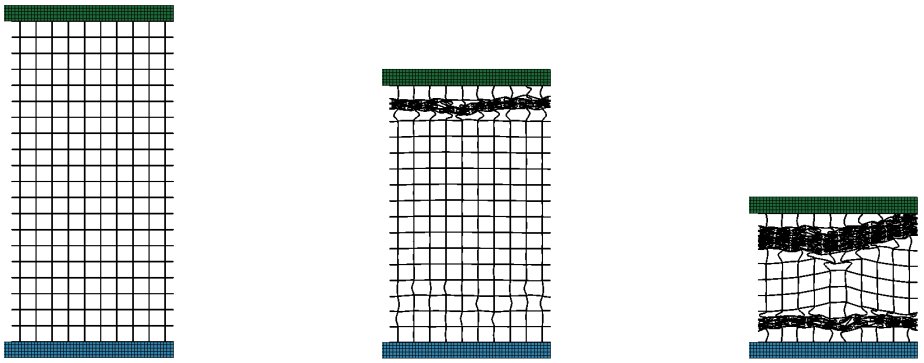

(a) $\varepsilon_{ave} = 0$ (b) $\varepsilon_{ave} = 0.2$ (c) $\varepsilon_{ave} = 0.6$

Figure 5. Deformation of cellular material with square cells of $\rho^*/\rho_s = 0.1$

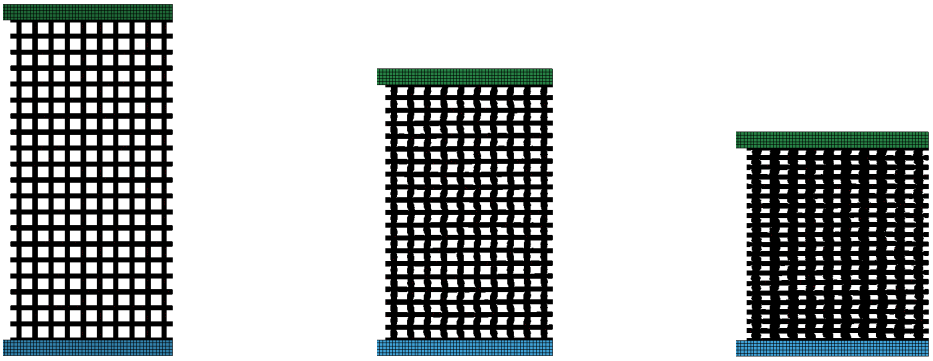

(a) $\varepsilon_{ave} = 0$ (b) $\varepsilon_{ave} = 0.2$ (c) $\varepsilon_{ave} = 0.4$

Figure 6. Deformation of cellular material with square cells of $\rho^*/\rho_s = 0.5$

Cellular materials with triangular cells generally collapse in a layer-by-layer pattern starting from both ends of the specimen as shown in Figure 7. Due to the truss-like structure, the impact force is transferred effectively from the impact end to the stationary end through axial force in the cell walls. Thus, the layer-by-layer collapse occurs due to buckling of the inclined cell walls which are under axial compression. Impact energy is absorbed through formation of plastic hinges along these buckled inclined cell walls. Buckling of cell walls within each layer of cells leads to load redistribution to adjacent cell layers which has not buckled, which results in the layer-by-layer collapse pattern observed in cellular materials with triangular cells.

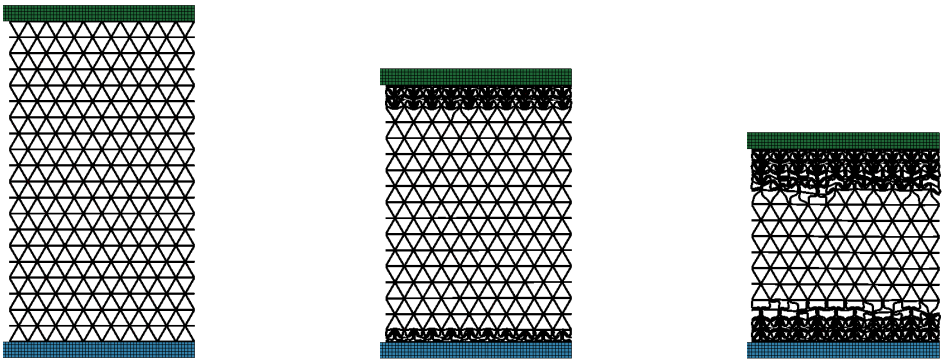

(a) $\varepsilon_{ave} = 0$ (b) $\varepsilon_{ave} = 0.2$ (c) $\varepsilon_{ave} = 0.4$

Figure 7. Deformation of cellular material with triangular cells of $\rho^*/\rho_s = 0.3$

3.2 Plateau stress, densification strain and impact energy absorption

As shown in Figure 8, cellular materials with square cells have the largest plateau stress followed by those with triangular cells, while the specimen with rhombic cells has the lowest plateau stress. As the cell walls cannot rotate easily about the joints for specimens with square and triangular cells, it is much harder for cell collapse to occur in these specimens prior to buckling of the cell walls. On the other hand, for cellular specimens with hexagonal and rhombic cell walls, the inclined cell walls can rotate easily about the joints. As there are no restraints to lateral deflection, cell collapse occurs more readily in the specimens with hexagonal and rhombic cells. Consequently, the cellular specimens with square and triangular cells are able to sustain larger plateau stress compared to those with hexagonal and rhombic cells.

The opposite trend is observed for densification strain (i.e. overall strain at the onset of global densification); the cellular specimen with square cells has the lowest densification strain, followed by those with triangular, hexagonal and rhombic cells. This is because the presence of the continuous horizontal cell walls restricts lateral deformation of the specimens with square and triangular cells, resulting in larger residual voids within collapsed cell layers. On the other hand, the voids within specimens with hexagonal and rhombic cells can be reduced to a much greater degree since the specimen is able to expand laterally. Consequently, the strain at which densification is reached is larger for these cases.

Therefore, as shown in Figure 8, cellular specimens with square cells has the greatest energy absorption capacity followed by the one with triangular, hexagonal and rhombic cells; this trend is similar to that observed earlier for the plateau stress. For the different cell shapes considered here, higher energy absorption capacity results from ability of the cellular materials to sustain larger plateau stress rather than having greater densification strain.

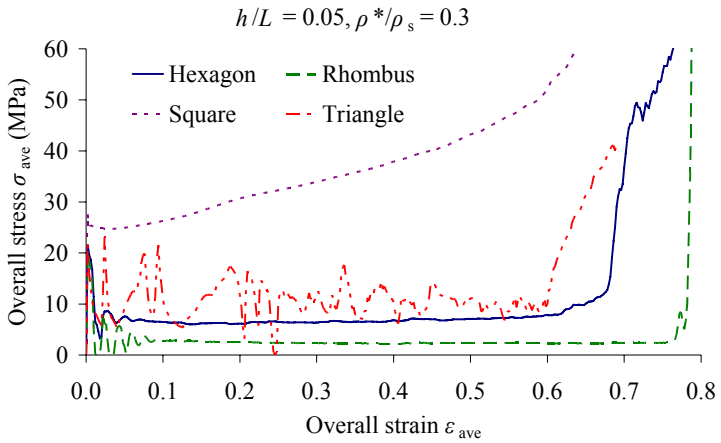

Figure 8. Overall stress-strain response of cellular materials of $\rho^*/\rho_s = 0.3$ with different cell shapes

4 Effect of base material ductility on overall response of cellular materials with different cell shapes

4.1 Hexagonal cells

Figures 3 and 9(a) show that deformation in cellular materials with hexagonal cells occurs through the formation of diagonal shear bands. Introducing ductility limit in terms of the base material rupture strain does not alter the formation of the shear bands within the specimen. However, damage (i.e. rupture of cell wall elements) is concentrated at the intersections of the shear bands as shown in Figure 9(c) while other regions of the specimen are relatively undeformed. This is because the maximum deformation occurs at the plastic hinges at intersections of the shear bands. Hence, the rupture strain is reached first at these locations. Moreover, damage in each cell wall begins from the plastic hinges at the joints since these are the regions with greatest deformation within each cell wall.

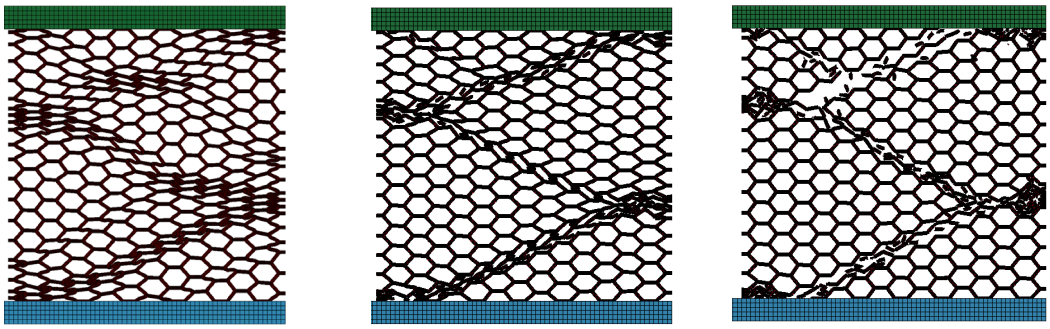

(a) ε_f = infinite (b) ε_f = 0.7 (c) ε_f = 0.3

Figure 9. Deformation of cellular material with hexagonal cells of $\rho^*/\rho_s = 0.3$ for different ε_f at $\varepsilon_{ave} = 0.4$

As damaged segments of the cell walls are unable to carry any load, stress redistribution occurs as the load is transferred from the damaged segments of the cell walls to neighbouring segments which are still intact. This stress redistribution leads to an increase in deformation in these neighbouring segments. For cellular materials which base material has a large ductility limit, stress redistribution can occur over significantly larger regions surrounding the damaged cell wall segments without causing further increase in the number of damaged cell wall segments. As a result, the overall collapse pattern and distribution of deformation within the specimen as shown in Figure 9(b) does not differ considerably from one with unlimited ductility as shown in Figure 9(a). On the other hand, the extent of stress redistribution for cellular materials which base material has a low ductility limit is very small. Stress redistribution from damaged cell walls segments causes almost immediate damage to neighbouring segments as well. Consequently, there is a rapid

increase in number of damaged cell wall segments (as indicated by the percentage of ruptured cell walls as shown in Figure 10(b)) but the damage is localized at the intersections of the shear bands as shown in Figure 9(c). Therefore, a higher rupture strain ε_f allows for more extensive stress distribution before further damage occurs in cellular materials with limited base material ductility.

Figure 10(a) shows that the plateau stress of a cellular material with hexagonal cells reduces with decreasing base material rupture strain ε_f. This is because damage of cell walls occurs more easily and extensively in cellular materials which base material has a low ductility limit due to limited stress redistribution after onset of damage. On the other hand, a smaller reduction in the plateau stress (with respect to the case without rupture in which ε_f is taken as infinite) is observed for cases with higher value of ε_f since extent of damage is more limited and the applied compression can be effectively resisted across larger regions of the specimen. Additionally, the onset of plateau stress reduction happens when the rupture strain is reached in some cell wall segments; the percentage of ruptured cell walls increases with overall strain as shown in Figure 10(b) as the damaged elements are deleted from the specimen. Since the failure strain is reached earlier in the cell walls of cellular materials with lower ductility limit, this onset of plateau stress reduction also occurs earlier. Therefore, since the plateau stress reduces with decreasing base material ductility, the energy absorption capacity of the material also reduces in the same manner.

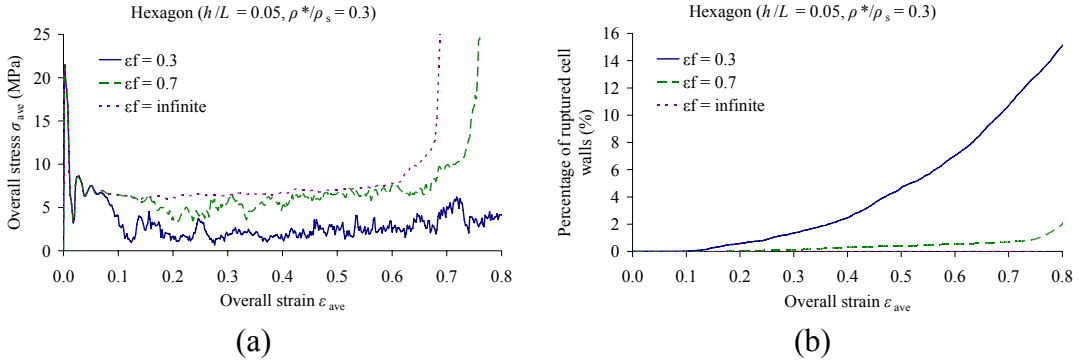

(a) (b)

Figure 10. (a) Overall stress-strain response, and (b) percentage of ruptured cell walls for cellular material with hexagonal cells of $\rho^*/\rho_s = 0.3$ for different ε_f

4.2 Rhombic cells

Figures 4 and 11(a) show that for elastic-perfectly plastic cellular materials with rhombic cells and infinite ductility, there is no clear formation of shear bands in the specimen; the material is rather evenly deformed throughout the specimen, with plastic hinges readily formed at the joints between cell walls. However, when the ductility limit of the base material is taken into account, a different overall failure mode is observed. As shown in Figure 11(c), diagonal bands are formed which

orientation with respect to the direction of compression follows that of the individual cells (i.e. at 45° with respect to direction of loading). Since there are not continuous horizontal cell walls, the cellular material can expand freely in the lateral direction when subjected to uniaxial compression. As the degree of lateral restraint increases from the cells along the free edge to those along the centre of the specimen (i.e. along the line of symmetry), the resistance of the former cells to the applied vertical compression is lower compared to the later. Consequently, the compression force applied on the cellular specimen increases across its width from the edges to the centre, with the resultant force acting at the centre (along the line of symmetry). Because of the unique shape and orientation of these rhombic cells with respect to the direction of loading, "super cells" can be formed across the entire specimen which shape and orientation are identical to the smaller constituent cells. The resultant applied compression force is transferred through the "walls" of the "super cells" in exactly the same manner as at the level of individual cells. As a result, the individual cells along these diagonal bands are subjected to a greater degree of deformation compared to cells in other regions of the specimen. This is evident in Fig. 12 which shows that rupture begins at the joints between cell walls that lie along the diagonal bands. In cellular materials with hexagonal cells, similar "super cells" are not formed in the specimen because the orientation of the diagonal bands is different from the angle of inclination of the diagonal cell walls.

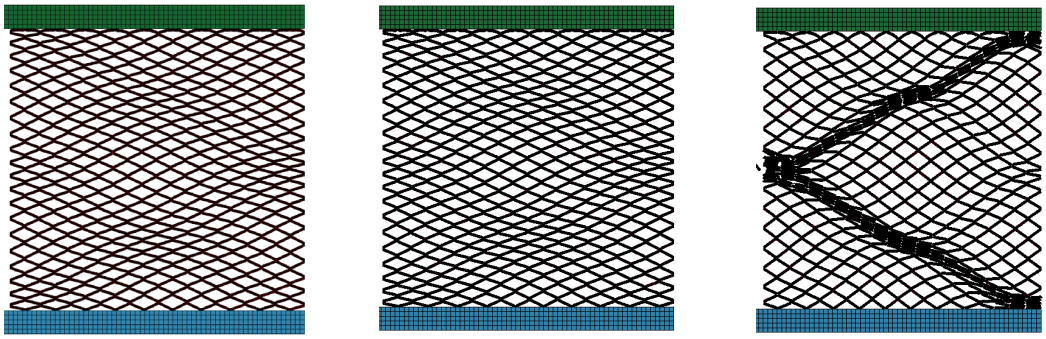

(a) ε_f = infinite (b) ε_f = 0.7 (c) ε_f = 0.3

Figure 11. Deformation of cellular material with rhombic cells of ρ^*/ρ_s = 0.3 for different ε_f at ε_{ave} = 0.4

For cellular materials which base material has a high ductility, the formation of these "super cells" or diagonal bands is not obvious because extensive stress redistribution can occur, whereby other cells which do not lie along the diagonal bands are also mobilized to resist the applied compression even as plastic hinges have been formed in the cells along the bands. This stress redistribution evens out the distribution of deformation and load resisted by the cells within the entire specimen, hence the formation of diagonal bands is not obvious as shown in Figures 11(a) and 11(b). However, in cases where the base material has a low ductility, the extent of stress redistribution is limited and damage is concentrated along the diagonal bands as shown in Figure 11(c).

Figure 13(a) shows that the plateau stress of a cellular material with rhombic cells also reduces with decreasing base material rupture strain ε_f. This is because of the higher number of damaged cell wall segments and greater extent of damage for cases with low values of ε_f, since stress redistribution after onset of damage is more limited. However, compared to cellular materials with hexagonal cells, those with rhombic cells seem to be less significantly affected by limited base material ductility. As shown in Figure 13(a), the onset of plateau stress reduction occurs at a larger applied overall strain ε_{ave} and the rate of decrease is more gradual. This is a result of the diagonal band formation, which occurs at a greater degree of applied compression in cellular materials with rhombic cells because of the smaller energy difference between deforming the rhombic cells in the principal versus inclined directions compared to that in cellular materials with hexagonal cells. Also, the number of damaged cell walls segments and extent of damage is lower for cellular materials with rhombic cells as shown in Figures 13(b) and 11 compared to those with hexagonal cells.

Therefore, since the plateau stress reduces with decreasing base material ductility, the energy absorption capacity of the material also reduces in the same manner.

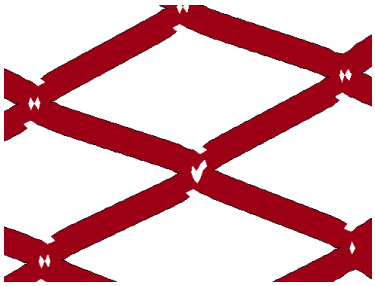

Figure 12. Damage of joints along the diagonal bands in cellular material with rhombic cells of $\rho^*/\rho_s = 0.3$ for $\varepsilon_f = 0.3$ at $\varepsilon_{ave} = 0.2$

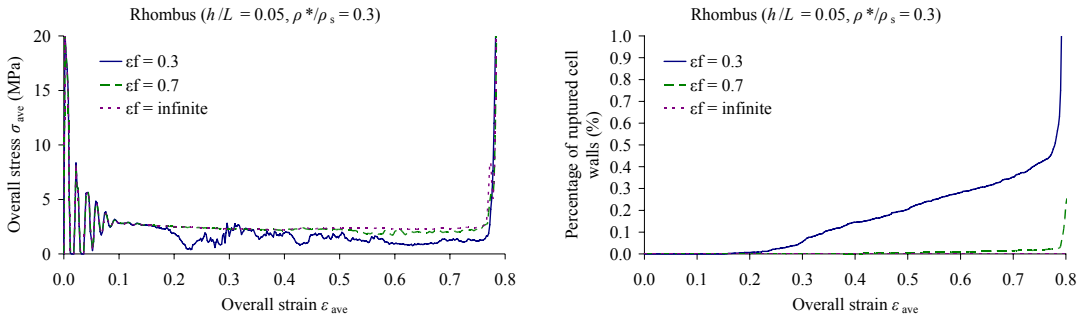

(a) (b)

Figure 13. (a) Overall stress-strain response, and (b) percentage of ruptured cell walls for cellular material with rhombic cells of $\rho^*/\rho_s = 0.3$ for different ε_f

4.3 Square cells

Figures 5 and 14(a) show that deformation of cellular materials with square cells and relative density of 0.1 initiates at both the impact and stationary ends of the specimen and a layer-by-layer collapse pattern is observed. The same process is observed in cases where the base material has limited ductility as shown in Figures 14(b) and 14(c). Figure 15(a) shows that the overall stress of a cellular material with square cells increases with increasing base material rupture strain ε_f. This is because of the greater degree of rotation which can be sustained at the plastic hinges (which are formed in the buckled cell walls) prior to damage. As shown in Figure 15(b), damage of cell walls (which can be represented by the percentage of ruptured cell walls) increases more rapidly with reducing base material ductility. Hence, the overall stress which can be sustained by the specimen is lower for cases with low base material ductility since damage occurs before rotational capacity of the buckled cell walls is reached. As a result, the energy absorption capacity also reduces with decreasing base material ductility.

On the other hand, Figures 6 and 16(a) show that deformation of cellular materials with square cells and relative density of 0.5 occurs through axial compression, i.e. squashing of the vertical cell walls, and is fairly uniform across the entire specimen for cases with unlimited base material ductility. However, for cases with limited base material ductility, a layer-by-layer collapse pattern is observed as shown in Figures 16(b) and 16(c) instead of a more uniform deformation. Localization happens when damage takes place in the first layer of cells, after which subsequent damage and collapse occur in the neighbouring cell layers due to load redistribution from the collapsed cell layers to adjacent layers which are still intact. While the location where localization of damage occurs is rather random – as this is sensitive to non-uniformity in the finite element mesh – the same layer-by-layer collapse pattern results after damage in the first layer of cells is initiated.

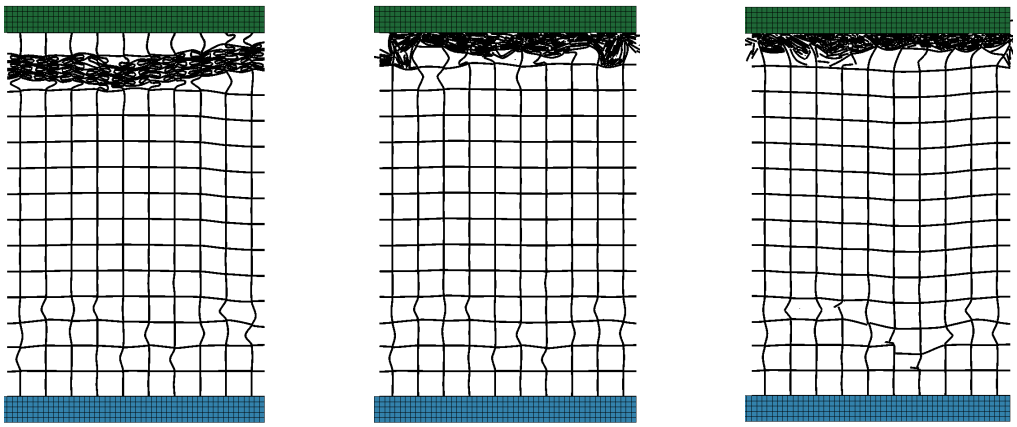

(a) ε_f = infinite (b) ε_f = 0.7 (c) ε_f = 0.3

Figure 14. Deformation of cellular material with square cells of $\rho^*/\rho_s = 0.1$ for different ε_f at $\varepsilon_{ave} = 0.3$

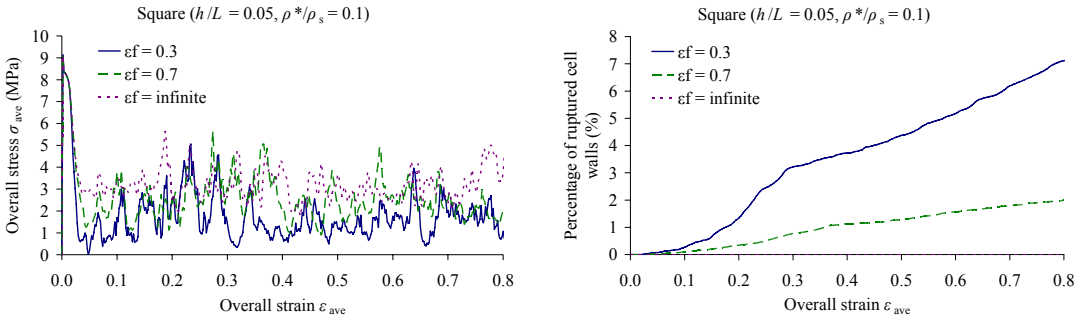

(a) (b)

Figure 15. (a) Overall stress-strain response, and (b) percentage of ruptured cell walls for cellular material with square cells of $\rho^*/\rho_s = 0.1$ for different ε_f

Because of this change in the collapse pattern, the overall stress of the cellular material also reduces with decreasing base material rupture strain ε_f as shown in Figure 17(a) due to the lower degree of compression or squashing which can be sustained by the vertical cell walls before damage occurs. As a result, the energy absorption capacity also reduces with decreasing base material ductility. Moreover, the onset of damage – which results in the sudden reduction in the overall stress as shown in Figure 17(a) and is represented by the onset of increase in percentage of ruptured cell walls as shown in Figure 17(b) – occurs earlier in cases with lower base material ductility since the failure strain is reached earlier. However, after the onset of damage, the rate at which damage propagates in a layer-by-layer manner does not seem to vary significantly with the ductility of the base material as shown in Figure 17(b). Hence, these results here suggest that for cellular materials with square cells, greater base material ductility delays the onset of damage and results in higher overall stress, but has little effect in reducing or slowing down the extent of damage once it has occurred in the first layer of cells.

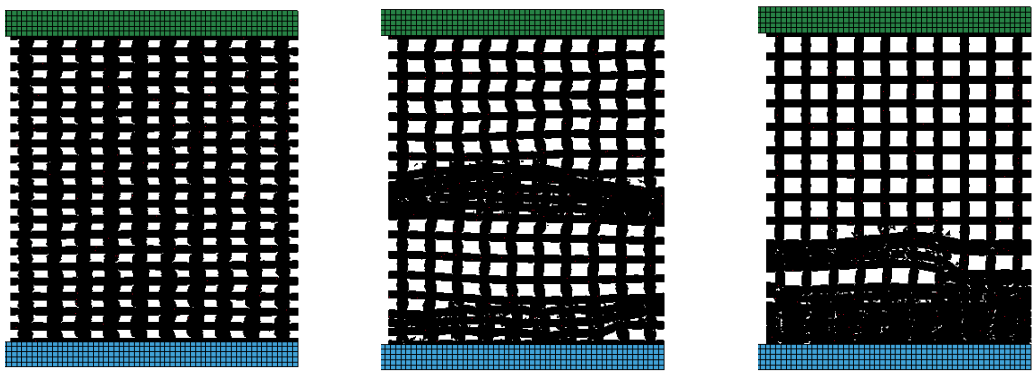

(a) ε_f = infinite (b) ε_f = 0.7 (c) ε_f = 0.3

Figure 16. Deformation of cellular material with square cells of $\rho^*/\rho_s = 0.5$ for different ε_f at $\varepsilon_{ave} = 0.4$

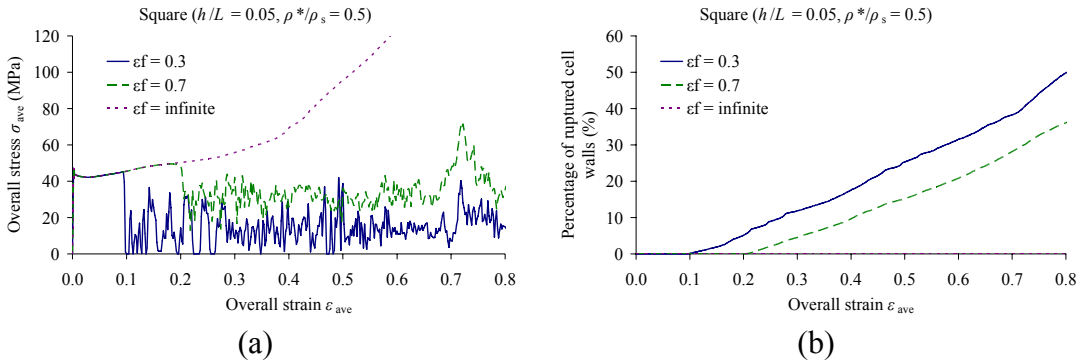

Figure 17. (a) Overall stress-strain response, and (b) percentage of ruptured cell walls for cellular material with square cells of $\rho^*/\rho_s = 0.5$ for different ε_f

4.4 Triangular cells

Figures 7 and 17(a) show that for cellular materials with triangular cells and infinite base material ductility, a general layer-by-layer collapse pattern is observed and failure occurs through buckling of the inclined cell walls. The same process is observed in cases where the base material has limited ductility as shown in Figures 17(b) and 17(c). However, the localization of damage occurs only at the impact end of the specimen with low base material ductility, while those with higher base material ductility show damaged zones at both impact and stationary ends. This is because in cases with low base material ductility, damage of the cell walls occurs earlier and limits the load which can be distributed from the cell layers near the impact end towards those near the stationary end. It is evident from Figure 18 that the degree of rotation which can be sustained by the buckled cell walls prior to damage is lower for the case with lower base material ductility.

As a result, the overall stress reduces while the extent of damage (which can be represented by the percentage of ruptured cell walls) increases with decreasing base material ductility as shown in Figure 19. Nevertheless, the reduction in the overall stress with decreasing base material ductility is not as significant for these cases with triangular cells compared to those with hexagonal and rhombic cells at the same relative density shown earlier in Figures 10 and 13. This is due to the fact that for cellular materials with triangular cells, the limited base material ductility does not alter the main mode of load resistance and cell wall failure, which is axial resistance that results in cell wall buckling. The base material ductility only changes the extent to which the post-buckling strength can be sustained, but in any case the cell walls lose most of their axial resistance once buckling has occurred. On the other hand, cellular materials with hexagonal and rhombic cells deform through rotation of plastic hinges formed at joints between cell walls. Since the rotational capacity of plastic hinges is proportional to the base material ductility, the resistance of these materials reduces more significantly with decreasing base material ductility.

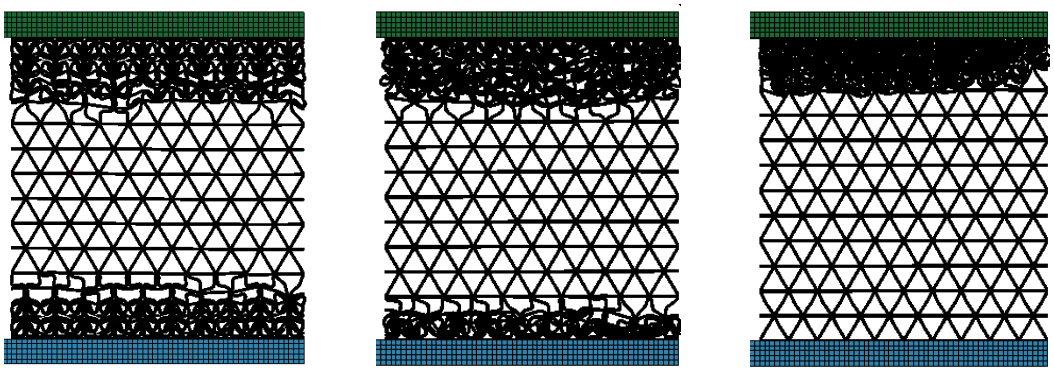

(a) ε_f = infinite (b) ε_f = 0.7 (c) ε_f = 0.3

Figure 17. Deformation of cellular material with triangular cells of $\rho^*/\rho_s = 0.3$ for different ε_f at $\varepsilon_{ave} = 0.4$

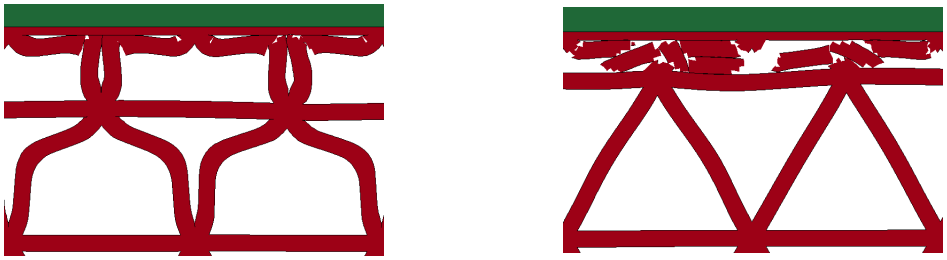

(a) ε_f = 0.7 (b) ε_f = 0.3

Figure 18. Deformation of cellular material with triangular cells of $\rho^*/\rho_s = 0.3$ for different ε_f at $\varepsilon_{ave} = 0.04$

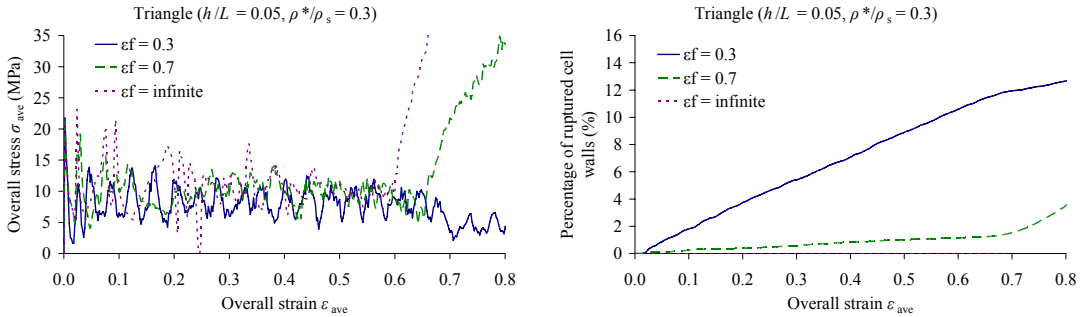

(a) (b)

Figure 19. (a) Overall stress-strain response, and (b) percentage of ruptured cell walls for cellular material with triangular cells of $\rho^*/\rho_s = 0.3$ for different ε_f

4.5 Plateau stress, impact energy absorption and extent of damage

As shown in Figure 20(a), when the effect of base material ductility is taken into account, cellular materials with square and triangular cells have larger plateau stress and energy absorption capacity compared with those with hexagonal and rhombic cells. This trend is similar to the results shown earlier in Figure 8 for cellular materials with unlimited base material ductility. This is because the main modes of load resistance and deformation are not affected by base material ductility. However, the magnitudes of the load resistance and energy absorption capacity reduce with decreasing base material ductility because of the lower axial strain in the cell walls and/or rotational capacity at the joints which can be sustained prior to damage.

Figure 20(b) shows that at the same relative density, the size of the damaged regions or the extent of damage (which can be represented by the percentage of ruptured cell walls) is generally highest for cellular materials with square cells, followed by those with triangular and hexagonal cells, and lowest for those with rhombic cells. This is because cellular materials with square cells tend to resist the impact force mainly through axial compression along entire lengths of the vertical cell walls. On the other hand, those with rhombic cells deform through rotation at the joints between the cell walls while the cell walls are relatively undeformed. Consequently, the extent of damage in cellular materials with square cells is larger because prior to buckling or damage the axial stresses along the vertical cells walls are rather uniform. However, for cellular materials with rhombic cells, the highly stressed regions are the joints about which rotation of the cell walls occurs. Therefore, the damaged zones in cellular materials with rhombic cells are smaller compared to those with other cell shapes.

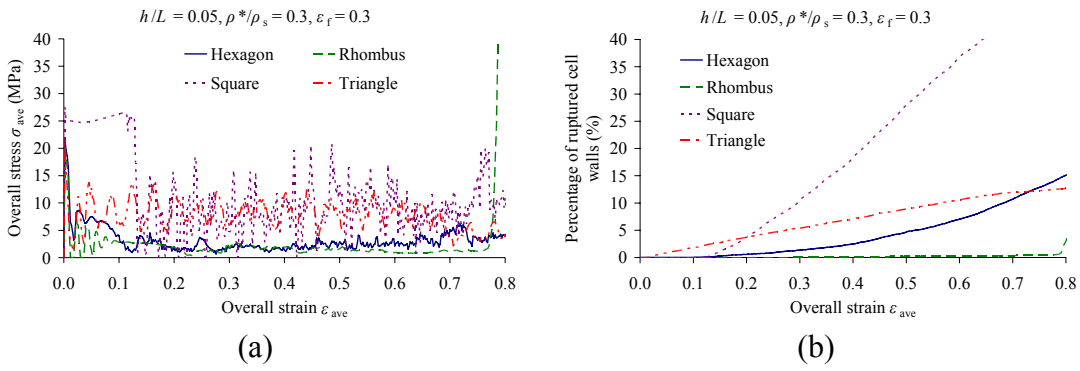

Figure 20. (a) Overall stress-strain response, and (b) percentage of ruptured cell walls for cellular materials of $\rho^*/\rho_s = 0.3$ and $\varepsilon_f = 0.3$ with different cell shapes

5 Effect of base material ductility on cellular materials with different relative densities

Figures 21 and 22 compare the effect of base material ductility on cellular materials with hexagonal cells of different relative densities. It is clear that the onset of overall stress reduction due to damage occurs at lower overall strain in specimens with low relative density. This is because these specimens have thinner cell walls which are more flexible, thus the failure strain is reached earlier. However, Figures 21(a) and 22(a) also show that the effect of base material ductility on the overall stress is much less significant for cellular materials with low relative density but becomes increasingly significant with increasing relative density. This is because for specimens with higher relative density, the size of the plastic zone and the force resisted by the material are greater. Consequently, when unloading occurs during damage of the cell walls, a greater reduction in the overall stress is observed. Moreover, the extent (i.e. size or area) damage zones – which can be represented by percentage of ruptured cell walls – is also greater with increasing relative density as shown in Figures 21(b) and 22(b).

The same trends are also observed for cellular materials with square cells as shown earlier in Figures 15 and 17. For specimens with low relative density in which the vertical cell walls fail through buckling, base material ductility changes only the extent to which the post-buckling strength can be sustained but does not affect the onset of buckling since the cell wall length-to-thickness ratio is unchanged. However, for specimens with high relative density in which the vertical cell walls fail through squashing or crushing, the vertical cell walls expand laterally due to axial compression. A greater base material ductility allows these cell walls to be compressed to a larger degree and hence a wider lateral expansion due to the Poisson effect. As a result, the maximum axial force which can be resisted by the cell walls increases since the cross-sectional area of the cell walls is increased. Consequently, when damage occurs and unloading happens, a greater reduction in the overall stress is observed. Therefore, the effect of base material ductility becomes increasingly significant with higher relative density.

6 Conclusions

In this paper, finite element simulations are carried out to investigate the effects of cell shape and base material ductility on the impact force and energy absorption capacity of metallic cellular materials with different relative densities under medium velocity impact. The results show that cell shape has a very significant influence on the overall response. At the same relative density, cellular specimens with square cells has the greatest overall stress and energy absorption capacity followed by those with triangular, hexagonal and rhombic cells. For these cellular materials with basic shapes higher energy absorption capacity typically results from ability of the cellular materials to sustain larger overall stress rather than having greater densification strain.

When the effect of base material ductility is taken into account, the overall stress and energy absorption capacity reduces with lower base material ductility. With lower base material ductility, more localized deformation patterns are observed due to less extensive load redistribution. Also, the effect of base material ductility on the overall response of the cellular materials is more significant in specimens with higher relative densities. However, the effect of cell shape on the overall response is not significantly altered even when base material ductility is taken into account because the primary modes of load resistance and energy absorption are unchanged.

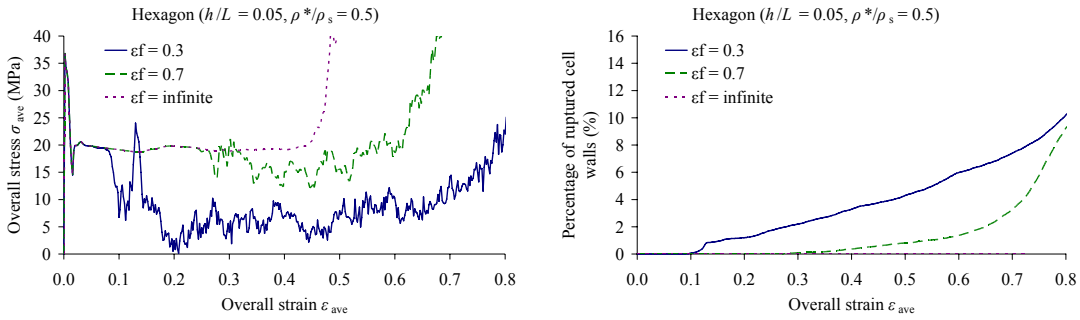

Figure 21. (a) Overall stress-strain response, and (b) percentage of ruptured cell walls for cellular material with hexagonal cells of $\rho^*/\rho_s = 0.5$ for different ε_f

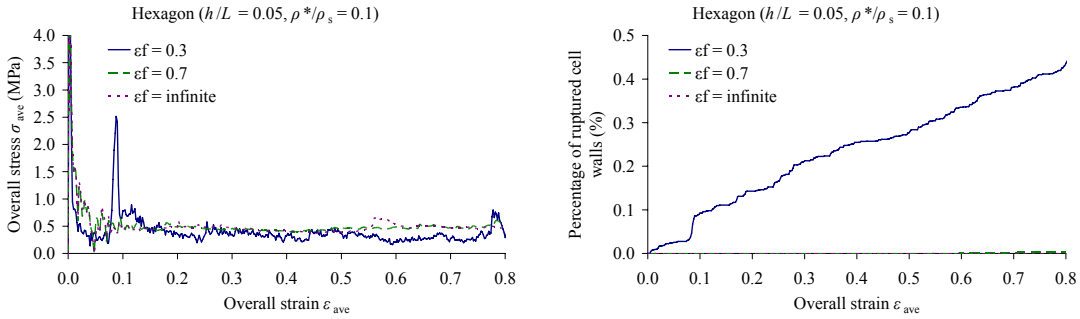

Figure 22. (a) Overall stress-strain response, and (b) percentage of ruptured cell walls for cellular material with hexagonal cells of $\rho^*/\rho_s = 0.1$ for different ε_f

References

[1] M. Ali, A. Qamhiyah, D. Flugard, M. Shakoor, "Theoretical and finite element study of a compact energy absorber", Advances in Engineering Software, 39, 95-106, 2008.

[2] M.A. Meyers, P.Y. Chen, A.Y.M. Lin, Y. Seki, "Biological materials: structure and mechanical properties", Progress in Materials Science, 53, 1-206, 2008.
[3] H. Rhee, M.F. Horstemeyer, Y. Hwang, H. Lim, H. El Kadiri, W. Trim, "A study on the structure and mechanical behaviour the *Terrapene carolina* carapace: a pathway to design bio-inspired synthetic composites", Materials Science and Engineering C, 29, 2333-2339, 2009.
[4] V.P.W. Shim, K.Y. Yap, "Modelling impact deformation of foam-plate sandwich systems", International Journal of Impact Engineering, 9, 615-636, 1997.
[5] H. Mahfuz, T. Thomas, V. Rangari, S. Jeelani, "On the dynamic response of sandwich composites and their core materials", Composites Science and Technology, 66, 2465-2472, 2006.
[6] C.J. Yungwirth, H.N.G. Wadley, J.H. O'Connor, A.J. Zakraysek, V.S. Deshpande, "Impact response of sandwich plates with a pyramidal lattice core", International Journal of Impact Engineering, 35, 920-936, 2008.
[7] W. Hou, F. Zhu, G. Lu, D.N. Fang, "Ballistic impact experiments of metallic sandwich panels with aluminum foam core", International Journal of Impact Engineering, 37, 1045-1055, 2010.
[8] L.J. Gibson, M.F. Ashby, "Cellular materials: structure and properties", second ed., Cambridge University Press, Cambridge, 1997.
[9] X.M. Qiu, J. Zhang, T.X. Yu, "Collapse of periodic planar lattices under uniaxial compression, part I: quasi-static strength predicted by limit analysis", International Journal of Impact Engineering, 36, 1223-1230, 2009.
[10] A.J. Wang, D.L. McDowell, "In-plane stiffness and yield strength of periodic metal honeycombs", Journal of Engineering Materials and Technology, 126, 137-156, 2004.
[11] X.J. Ren, V.V. Silberschmidt, "Numerical modelling of low-density cellular materials", Computational Materials Science, 43, 65-74, 2008.
[12] X.M. Qiu, J. Zhang, T.X. Yu, "Collapse of periodic planar lattices under uniaxial compression, part II: dynamic crushing based on finite element simulation", International Journal of Impact Engineering, 36, 1231-1241, 2009.
[13] K. Li, X.-L. Gao, J. Wang, "Dynamic crushing behaviour of honeycomb structures with irregular cell shapes and non-uniform cell wall thickness", International Journal of Solids and Structures, 44, 5003-5026, 2007.
[14] A. Ajdari, H. Nayeb-Hashemi, A. Vaziri, "Dynamic crushing and energy absorption of regular, irregular and functionally graded cellular structures", International Journal of Solids and Structures, 48, 506-516, 2011.
[15] X.-C. Zhang, Y. Liu, B. Wang, Z.-M. Zhang, "Effects of defects on the in-plane dynamic crushing of metal honeycombs", International Journal of Mechanical Sciences, 52, 1290-1298, 2010.
[16] N. Jones, "Structural impact", Cambridge University Press, Cambridge: New York, 1989.